19. STRUCTURE FUNCTIONS

Updated September 2013 by B. Foster (University of Hamburg/DESY), A.D. Martin (University of Durham), and M.G. Vincter (Carleton University).

19.1. Deep inelastic scattering

High-energy lepton-nucleon scattering (deep inelastic scattering) plays a key role in determining the partonic structure of the proton. The process $\ell N \to \ell' X$ is illustrated in Fig. 19.1. The filled circle in this figure represents the internal structure of the proton which can be expressed in terms of structure functions.

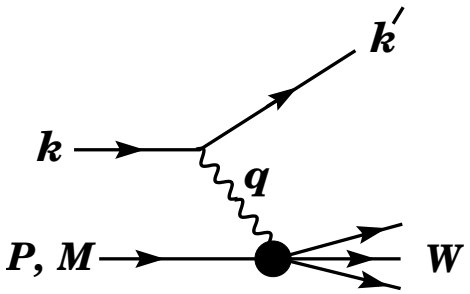

Figure 19.1: Kinematic quantities for the description of deep inelastic scattering. The quantities k and k' are the four-momenta of the incoming and outgoing leptons, P is the four-momentum of a nucleon with mass M, and W is the mass of the recoiling system X. The exchanged particle is a γ, $W^{\pm}$, or Z; it transfers four-momentum $q = k - k'$ to the nucleon.

Invariant quantities:

$\nu = \dfrac{q \cdot P}{M} = E - E'$ is the lepton's energy loss in the nucleon rest frame (in earlier literature sometimes $\nu = q \cdot P$). Here, E and E' are the initial and final lepton energies in the nucleon rest frame.

$Q^2 = -q^2 = 2(EE' - \vec{k} \cdot \vec{k}') - m_\ell^2 - m_{\ell'}^2$ where $m_\ell(m_{\ell'})$ is the initial (final) lepton mass. If $EE' \sin^2(\theta/2) \gg m_\ell^2,\ m_{\ell'}^2$, then

$\approx 4EE' \sin^2(\theta/2)$, where θ is the lepton's scattering angle with respect to the lepton beam direction.

$x = \dfrac{Q^2}{2M\nu}$ where, in the parton model, x is the fraction of the nucleon's momentum carried by the struck quark.

$y = \dfrac{q \cdot P}{k \cdot P} = \dfrac{\nu}{E}$ is the fraction of the lepton's energy lost in the nucleon rest frame.

$W^2 = (P + q)^2 = M^2 + 2M\nu - Q^2$ is the mass squared of the system X recoiling against the scattered lepton.

$s = (k + P)^2 = \dfrac{Q^2}{xy} + M^2 + m_\ell^2$ is the center-of-mass energy squared of the lepton-nucleon system.

The process in Fig. 19.1 is called deep ($Q^2 \gg M^2$) inelastic ($W^2 \gg M^2$) scattering (DIS). In what follows, the masses of the initial and scattered leptons, m_ℓ and $m_{\ell'}$, are neglected.

19.1.1. ***DIS cross sections*** :

The double-differential cross section for deep inelastic scattering can be expressed in terms of kinematic variables in several ways.

$$\frac{d^2\sigma}{dx\,dy} = x\,(s - M^2)\,\frac{d^2\sigma}{dx\,dQ^2} = \frac{2\pi\,M\nu}{E'}\frac{d^2\sigma}{d\Omega_{\rm Nrest}\,dE'}\ . \tag{19.1}$$

In lowest-order perturbation theory, the cross section for the scattering of polarized leptons on polarized nucleons can be expressed in terms of the products of leptonic and hadronic tensors associated with the coupling of the exchanged bosons at the upper and lower vertices in Fig. 19.1 (see Refs. 1–4)

$$\frac{d^2\sigma}{dxdy} \;=\; \frac{2\pi y\alpha^2}{Q^4}\;\sum_j\;\eta_j\;L_j^{\mu\nu}\;W^j_{\mu\nu}\ . \tag{19.2}$$

For neutral-current processes, the summation is over $j = \gamma, Z$ and γZ representing photon and Z exchange and the interference between them, whereas for charged-current interactions there is only W exchange, $j = W$. (For transverse nucleon polarization, there is a dependence on the azimuthal angle of the scattered lepton.) The lepton tensor $L_{\mu\nu}$ is associated with the coupling of the exchange boson to the leptons. For incoming leptons of charge $e = \pm 1$ and helicity $\lambda = \pm 1$,

$$\begin{aligned}
L^\gamma_{\mu\nu} &= 2\left(k_\mu k'_\nu + k'_\mu k_\nu - (k\cdot k' - m_\ell^2)g_{\mu\nu} - i\lambda\varepsilon_{\mu\nu\alpha\beta}k^\alpha k'^\beta\right),\\
L^{\gamma Z}_{\mu\nu} &= (g_V^e + e\lambda g_A^e)\;L^\gamma_{\mu\nu}, \qquad L^Z_{\mu\nu} = (g_V^e + e\lambda g_A^e)^2\;L^\gamma_{\mu\nu},\\
L^W_{\mu\nu} &= (1 + e\lambda)^2\;L^\gamma_{\mu\nu},
\end{aligned} \tag{19.3}$$

where $g_V^e = -\frac{1}{2} \;+\; 2\sin^2\theta_W, \qquad g_A^e \;=\; -\frac{1}{2}$.

Although here the helicity formalism is adopted, an alternative approach is to express the tensors in Eq. (19.3) in terms of the polarization of the lepton.

The factors η_j in Eq. (19.2) denote the ratios of the corresponding propagators and couplings to the photon propagator and coupling squared

$$\begin{aligned}
\eta_\gamma \;&=\; 1 \quad ; \quad \eta_{\gamma Z} \;=\; \left(\frac{G_F M_Z^2}{2\sqrt{2}\pi\alpha}\right)\;\left(\frac{Q^2}{Q^2 + M_Z^2}\right);\\
\eta_Z \;&=\; \eta^2_{\gamma Z} \quad ; \quad \eta_W \;=\; \tfrac{1}{2}\left(\frac{G_F M_W^2}{4\pi\alpha}\;\frac{Q^2}{Q^2 + M_W^2}\right)^2 .
\end{aligned} \tag{19.4}$$

The hadronic tensor, which describes the interaction of the appropriate electroweak currents with the target nucleon, is given by

$$W_{\mu\nu} \;=\; \frac{1}{4\pi} \int d^4z\, e^{iq\cdot z} \,\left\langle P,S \left| \left[J^\dagger_\mu(z), J_\nu(0) \right] \right| \, P,S \right\rangle , \tag{19.5}$$

where S denotes the nucleon-spin 4-vector, with $S^2 = -M^2$ and $S\cdot P = 0$.

19.2. Structure functions of the proton

The structure functions are defined in terms of the hadronic tensor (see Refs. 1–3)

$$\begin{aligned} W_{\mu\nu} = & \left(-g_{\mu\nu} \;+\; \frac{q_\mu q_\nu}{q^2} \right) \, F_1(x,Q^2) + \frac{\hat{P}_\mu \hat{P}_\nu}{P\cdot q} \, F_2(x,Q^2) \\ & -\; i\varepsilon_{\mu\nu\alpha\beta} \, \frac{q^\alpha P^\beta}{2P\cdot q} \, F_3(x,Q^2) \\ & +\; i\varepsilon_{\mu\nu\alpha\beta} \, \frac{q^\alpha}{P\cdot q} \, \left[S^\beta g_1(x,Q^2) + \left(S^\beta \;-\; \frac{S\cdot q}{P\cdot q} \, P^\beta \right) \, g_2(x,Q^2) \right] \\ & +\; \frac{1}{P\cdot q} \, \left[\tfrac{1}{2} \left(\hat{P}_\mu \hat{S}_\nu \;+\; \hat{S}_\mu \hat{P}_\nu \right) - \frac{S\cdot q}{P\cdot q} \, \hat{P}_\mu \hat{P}_\nu \right] \, g_3(x,Q^2) \\ & +\; \frac{S\cdot q}{P\cdot q} \, \left[\frac{\hat{P}_\mu \hat{P}_\nu}{P\cdot q} \, g_4(x,Q^2) + \left(-g_{\mu\nu} \;+\; \frac{q_\mu q_\nu}{q^2} \right) \, g_5(x,Q^2) \right] \end{aligned} \tag{19.6}$$

where

$$\hat{P}_\mu \;=\; P_\mu \;-\; \frac{P\cdot q}{q^2} \, q_\mu, \qquad \hat{S}_\mu \;=\; S_\mu \;-\; \frac{S\cdot q}{q^2} \, q_\mu \; . \tag{19.7}$$

In Ref. 2, the definition of $W_{\mu\nu}$ with $\mu \leftrightarrow \nu$ is adopted, which changes the sign of the $\varepsilon_{\mu\nu\alpha\beta}$ terms in Eq. (19.6), although the formulae given below are unchanged. Ref. 1 tabulates the relation between the structure functions defined in Eq. (19.6) and other choices available in the literature.

The cross sections for neutral- and charged-current deep inelastic scattering on unpolarized nucleons can be written in terms of the structure functions in the generic form

$$\begin{aligned} \frac{d^2\sigma^i}{dxdy} \;=\; & \frac{4\pi\alpha^2}{xyQ^2} \, \eta^i \left\{ \left(1 \;-\; y \;-\; \frac{x^2y^2M^2}{Q^2} \right) \, F_2^i \right. \\ & \left. + \, y^2 x F_1^i \;\mp\; \left(y \;-\; \frac{y^2}{2} \right) \, x F_3^i \right\}, \end{aligned} \tag{19.8}$$

where i = NC, CC corresponds to neutral-current ($eN \to eX$) or charged-current ($eN \to \nu X$ or $\nu N \to eX$) processes, respectively. For incoming neutrinos, $L^W_{\mu\nu}$ of

Eq. (19.3) is still true, but with e, λ corresponding to the outgoing charged lepton. In the last term of Eq. (19.8), the $-$ sign is taken for an incoming e^+ or $\overline{\nu}$ and the $+$ sign for an incoming e^- or ν. The factor $\eta^{\rm NC} = 1$ for unpolarized $e^\pm$ beams, whereas*

$$\eta^{\rm CC} \;=\; (1 \pm \lambda)^2 \eta_W \tag{19.9}$$

with $\pm$ for $\ell^\pm$; and where λ is the helicity of the incoming lepton and η_W is defined in Eq. (19.4); for incoming neutrinos $\eta^{\rm CC} = 4\eta_W$. The CC structure functions, which derive exclusively from W exchange, are

$$F_1^{\rm CC} = F_1^W,\; F_2^{\rm CC} = F_2^W,\; xF_3^{\rm CC} = xF_3^W. \tag{19.10}$$

The NC structure functions $F_2^\gamma, F_2^{\gamma Z}, F_2^Z$ are, for $e^\pm N \to e^\pm X$, given by Ref. 5,

$$F_2^{\rm NC} \;=\; F_2^\gamma \;-\; (g_V^e \pm \lambda g_A^e)\eta_{\gamma Z} F_2^{\gamma Z} \;+\; ({g_V^e}^2 + {g_A^e}^2 \pm 2\lambda g_V^e g_A^e)\,\eta_Z F_2^Z \tag{19.11}$$

and similarly for $F_1^{\rm NC}$, whereas

$$xF_3^{\rm NC} = \; -(g_A^e \pm \lambda g_V^e)\eta_{\gamma Z} xF_3^{\gamma Z} + [2g_V^e g_A^e \pm \lambda({g_V^e}^2 + {g_A^e}^2)]\eta_Z xF_3^Z \;. \tag{19.12}$$

The polarized cross-section difference

$$\Delta\sigma \;=\; \sigma(\lambda_n = -1, \lambda_\ell) \;-\; \sigma(\lambda_n = 1, \lambda_\ell)\;, \tag{19.13}$$

where λ_ℓ, λ_n are the helicities (± 1) of the incoming lepton and nucleon, respectively, may be expressed in terms of the five structure functions $g_{1,\ldots 5}(x, Q^2)$ of Eq. (19.6). Thus,

$$\begin{aligned}
\frac{d^2\Delta\sigma^i}{dxdy} \;=\; & \frac{8\pi\alpha^2}{xyQ^2}\,\eta^i \left\{ -\lambda_\ell y \left(2 - y - 2x^2y^2\frac{M^2}{Q^2}\right)\; x g_1^i + \lambda_\ell 4x^3y^2\;\frac{M^2}{Q^2}\; g_2^i \right. \\
& +\; 2x^2 y \frac{M^2}{Q^2}\left(1 - y - x^2y^2\frac{M^2}{Q^2}\right)\; g_3^i \\
& \left. -\; \left(1 + 2x^2y\frac{M^2}{Q^2}\right)\left[\left(1 - y - x^2y^2\frac{M^2}{Q^2}\right)\; g_4^i + xy^2 g_5^i\right]\right\}
\end{aligned} \tag{19.14}$$

with $i =$ NC or CC as before. The Eq. (19.13) corresponds to the difference of antiparallel minus parallel spins of the incoming particles for e^- or ν initiated reactions, but the difference of parallel minus antiparallel for e^+ or $\overline{\nu}$ initiated processes. For longitudinal nucleon polarization, the contributions of g_2 and g_3 are suppressed by powers of M^2/Q^2. These structure functions give an unsuppressed contribution to the cross section for transverse polarization [1], but in this case the cross-section difference vanishes as $M/Q \to 0$.

Because the same tensor structure occurs in the spin-dependent and spin-independent parts of the hadronic tensor of Eq. (19.6) in the $M^2/Q^2 \to 0$ limit, the differential

cross-section difference of Eq. (19.14) may be obtained from the differential cross section Eq. (19.8) by replacing

$$F_1 \;\to\; -g_5 \;, \quad F_2 \;\to\; -g_4 \;, \quad F_3 \;\to\; 2g_1 \;, \tag{19.15}$$

and multiplying by two, since the total cross section is the average over the initial-state polarizations. In this limit, Eq. (19.8) and Eq. (19.14) may be written in the form

$$\begin{aligned} \frac{d^2\sigma^i}{dxdy} &= \frac{2\pi\alpha^2}{xyQ^2}\,\eta^i\left[Y_+F_2^i \mp Y_-xF_3^i - y^2F_L^i\right], \\ \frac{d^2\Delta\sigma^i}{dxdy} &= \frac{4\pi\alpha^2}{xyQ^2}\,\eta^i\left[-Y_+g_4^i \mp Y_-2xg_1^i + y^2g_L^i\right], \end{aligned} \tag{19.16}$$

with $i =$ NC or CC, where $Y_\pm = 1 \pm (1-y)^2$ and

$$F_L^i \;=\; F_2^i \;-\; 2xF_1^i \;, \qquad g_L^i \;=\; g_4^i \;-\; 2xg_5^i \;. \tag{19.17}$$

In the naive quark-parton model, the analogy with the Callan-Gross relations [6] $F_L^i = 0$, are the Dicus relations [7] $g_L^i = 0$. Therefore, there are only two independent polarized structure functions: g_1 (parity conserving) and g_5 (parity violating), in analogy with the unpolarized structure functions F_1 and F_3.

19.2.1. *Structure functions in the quark-parton model* :

In the quark-parton model [8,9], contributions to the structure functions F^i and g^i can be expressed in terms of the quark distribution functions $q(x,Q^2)$ of the proton, where $q = u, \overline{u}, d, \overline{d}$ etc. The quantity $q(x,Q^2)dx$ is the number of quarks (or antiquarks) of designated flavor that carry a momentum fraction between x and $x+dx$ of the proton's momentum in a frame in which the proton momentum is large.

For the neutral-current processes $ep \to eX$,

$$\begin{aligned} \left[F_2^\gamma,\; F_2^{\gamma Z},\; F_2^Z\right] &= x\sum_q \left[e_q^2,\; 2e_qg_V^q,\; {g_V^q}^2 + {g_A^q}^2\right]\;(q+\overline{q})\;, \\ \left[F_3^\gamma,\; F_3^{\gamma Z},\; F_3^Z\right] &= \sum_q \left[0,\; 2e_qg_A^q,\; 2g_V^qg_A^q\right]\;(q-\overline{q})\;, \\ \left[g_1^\gamma,\; g_1^{\gamma Z},\; g_1^Z\right] &= \tfrac{1}{2}\sum_q \left[e_q^2,\; 2e_qg_V^q,\; {g_V^q}^2 + {g_A^q}^2\right]\;(\Delta q+\Delta\overline{q})\;, \\ \left[g_5^\gamma,\; g_5^{\gamma Z},\; g_5^Z\right] &= \sum_q \left[0,\; e_qg_A^q,\; g_V^qg_A^q\right]\;(\Delta q-\Delta\overline{q})\;, \end{aligned} \tag{19.18}$$

where $g_V^q = \pm\frac{1}{2} - 2e_q\sin^2\theta_W$ and $g_A^q = \pm\frac{1}{2}$, with $\pm$ according to whether q is a $u-$ or $d-$type quark respectively. The quantity Δq is the difference $q\uparrow - q\downarrow$ of the distributions with the quark spin parallel and antiparallel to the proton spin.

For the charged-current processes $e^- p \to \nu X$ and $\overline{\nu} p \to e^+ X$, the structure functions are:

$$\begin{aligned} F_2^{W^-} &= 2x(u + \overline{d} + \overline{s} + c \ldots) \ , \\ F_3^{W^-} &= 2(u - \overline{d} - \overline{s} + c \ldots) \ , \\ g_1^{W^-} &= (\Delta u + \Delta \overline{d} + \Delta \overline{s} + \Delta c \ldots) \ , \\ g_5^{W^-} &= (-\Delta u + \Delta \overline{d} + \Delta \overline{s} - \Delta c \ldots) \ , \end{aligned} \tag{19.19}$$

where only the active flavors have been kept and where CKM mixing has been neglected. For $e^+ p \to \overline{\nu} X$ and $\nu p \to e^- X$, the structure functions F^{W^+}, g^{W^+} are obtained by the flavor interchanges $d \leftrightarrow u, s \leftrightarrow c$ in the expressions for F^{W^-}, g^{W^-}. The structure functions for scattering on a neutron are obtained from those of the proton by the interchange $u \leftrightarrow d$. For both the neutral- and charged-current processes, the quark-parton model predicts $2xF_1^i = F_2^i$ and $g_4^i = 2xg_5^i$.

Neglecting masses, the structure functions g_2 and g_3 contribute only to scattering from transversely polarized nucleons (for which $S \cdot q = 0$), and have no simple interpretation in terms of the quark-parton model. They arise from off-diagonal matrix elements $\langle P, \lambda' | [J_\mu^\dagger(z), J_\nu(0)] | P, \lambda \rangle$, where the proton helicities satisfy $\lambda' \neq \lambda$. In fact, the leading-twist contributions to both g_2 and g_3 are both twist-2 and twist-3, which contribute at the same order of Q^2. The Wandzura-Wilczek relation [10] expresses the twist-2 part of g_2 in terms of g_1 as

$$g_2^i(x) \ = \ -g_1^i(x) \ + \ \int_x^1 \ \frac{dy}{y} \ g_1^i(y) \ . \tag{19.20}$$

However, the twist-3 component of g_2 is unknown. Similarly, there is a relation expressing the twist-2 part of g_3 in terms of g_4. A complete set of relations, including M^2/Q^2 effects, can be found in Ref. 11.

19.2.2. *Structure functions and QCD* :

One of the most striking predictions of the quark-parton model is that the structure functions F_i, g_i *scale*, i.e., $F_i(x, Q^2) \to F_i(x)$ in the Bjorken limit that Q^2 and $\nu \to \infty$ with x fixed [12]. This property is related to the assumption that the transverse momentum of the partons in the infinite-momentum frame of the proton is small. In QCD, however, the radiation of hard gluons from the quarks violates this assumption, leading to logarithmic scaling violations, which are particularly large at small x, see Fig. 19.2. The radiation of gluons produces the evolution of the structure functions. As Q^2 increases, more and more gluons are radiated, which in turn split into $q\overline{q}$ pairs. This process leads both to the softening of the initial quark momentum distributions and to the growth of the gluon density and the $q\overline{q}$ sea as x decreases.

In QCD, the above process is described in terms of scale-dependent parton distributions $f_a(x, \mu^2)$, where $a = g$ or q and, typically, μ is the scale of the probe Q. For $Q^2 \gg M^2$, the structure functions are of the form

$$F_i = \sum_a C_i^a \otimes f_a, \tag{19.21}$$

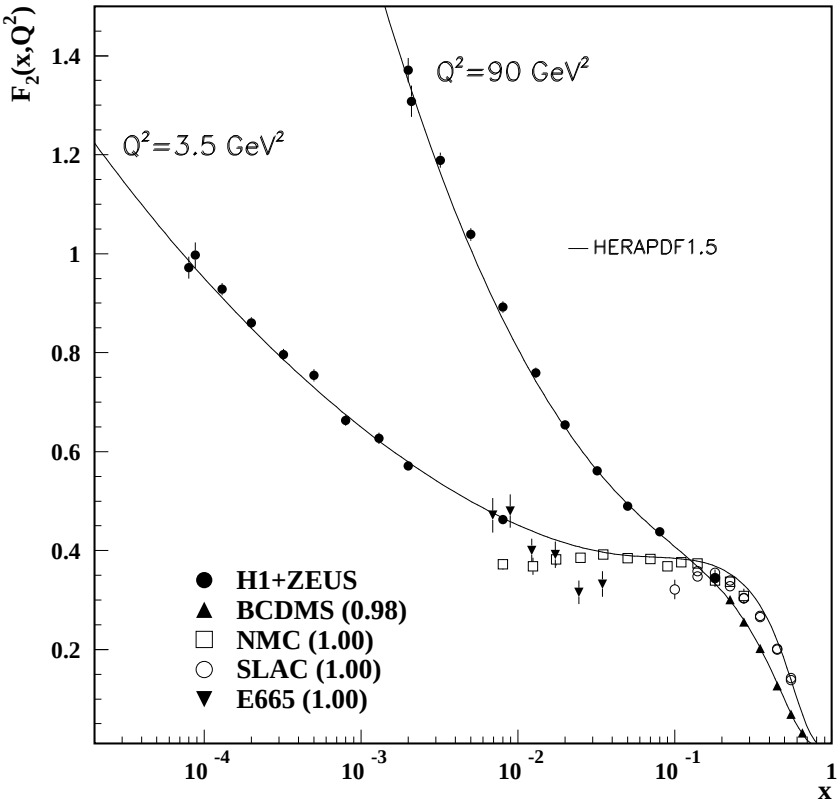

Figure 19.2: The proton structure function F_2^p given at two Q^2 values (3.5 GeV^2 and 90 GeV^2), which exhibit scaling at the 'pivot' point $x \sim 0.14$. See the captions in Fig. 19.8 and Fig. 19.10 for the references of the data. The various data sets have been renormalized by the factors shown in brackets in the key to the plot, which were globally determined in the full HERAPDF analysis [13]. In practice, data for the reduced cross section, $F_2(x,Q^2) - (y^2/Y_+)F_L(x,Q^2)$, are fitted, rather than F_2 and F_L separately.

where $\otimes$ denotes the convolution integral

$$C \otimes f = \int_x^1 \frac{dy}{y} C(y) f\left(\frac{x}{y}\right) , \tag{19.22}$$

and where the coefficient functions C_i^a are given as a power series in α_s. The parton distribution f_a corresponds, at a given x, to the density of parton a in the proton integrated over transverse momentum k_t up to μ. Its evolution in μ is described in QCD by a DGLAP equation (see Refs. 14–17) which has the schematic form

$$\frac{\partial f_a}{\partial \ln \mu^2} \sim \frac{\alpha_s(\mu^2)}{2\pi} \sum_b (P_{ab} \otimes f_b) , \tag{19.23}$$

where the P_{ab}, which describe the parton splitting $b \to a$, are also given as a power series in α_s. Although perturbative QCD can predict, via Eq. (19.23), the evolution of the

parton distribution functions from a particular scale, μ_0, these DGLAP equations cannot predict them *a priori* at any particular μ_0. Thus they must be measured at a starting point μ_0 before the predictions of QCD can be compared to the data at other scales, μ. In general, all observables involving a hard hadronic interaction (such as structure functions) can be expressed as a convolution of calculable, process-dependent coefficient functions and these universal parton distributions, e.g. Eq. (19.21).

It is often convenient to write the evolution equations in terms of the gluon, non-singlet (q^{NS}) and singlet (q^S) quark distributions, such that

$$q^{NS} \;=\; q_i - \overline{q}_i \quad (\text{or } \; q_i - q_j), \qquad q^S \;=\; \sum_i (q_i + \overline{q}_i) \; . \tag{19.24}$$

The non-singlet distributions have non-zero values of flavor quantum numbers, such as isospin and baryon number. The DGLAP evolution equations then take the form

$$\begin{aligned} \frac{\partial q^{NS}}{\partial \ln \mu^2} &= \frac{\alpha_s(\mu^2)}{2\pi} \, P_{qq} \;\otimes\; q^{NS} \; , \\ \frac{\partial}{\partial \ln \mu^2} \begin{pmatrix} q^S \\ g \end{pmatrix} &= \frac{\alpha_s(\mu^2)}{2\pi} \begin{pmatrix} P_{qq} & 2n_f \, P_{qg} \\ P_{gq} & P_{gg} \end{pmatrix} \otimes \begin{pmatrix} q^S \\ g \end{pmatrix} , \end{aligned} \tag{19.25}$$

where P are splitting functions that describe the probability of a given parton splitting into two others, and n_f is the number of (active) quark flavors. The leading-order Altarelli-Parisi [16] splitting functions are

$$P_{qq} = \tfrac{4}{3} \left[\frac{1+x^2}{(1-x)} \right]_+ = \tfrac{4}{3} \left[\frac{1+x^2}{(1-x)_+} \right] + 2\delta(1-x) \; , \tag{19.26}$$

$$P_{qg} = \tfrac{1}{2} \left[x^2 + (1-x)^2 \right] \; , \tag{19.27}$$

$$P_{gq} = \tfrac{4}{3} \left[\frac{1+(1-x)^2}{x} \right] \; , \tag{19.28}$$

$$\begin{aligned} P_{gg} = 6 \left[\frac{1-x}{x} + x(1-x) + \frac{x}{(1-x)_+} \right] \\ + \left[\frac{11}{2} - \frac{n_f}{3} \right] \delta(1-x), \end{aligned} \tag{19.29}$$

where the notation $[F(x)]_+$ defines a distribution such that for any sufficiently regular test function, $f(x)$,

$$\int_0^1 dx f(x) [F(x)]_+ = \int_0^1 dx \; (f(x) - f(1)) F(x) \; . \tag{19.30}$$

In general, the splitting functions can be expressed as a power series in α_s. The series contains both terms proportional to $\ln \mu^2$ and to $\ln \; 1/x$. The leading-order DGLAP

evolution sums up the $(\alpha_s \ln \mu^2)^n$ contributions, while at next-to-leading order (NLO) the sum over the $\alpha_s(\alpha_s \ln \mu^2)^{n-1}$ terms is included [18,19]. In fact, the NNLO contributions to the splitting functions and the DIS coefficient functions are now also all known [20–22].

In the kinematic region of very small x, it is essential to sum leading terms in $\ln\ 1/x$, independent of the value of $\ln \mu^2$. At leading order, LLx, this is done by the BFKL equation for the unintegrated distributions (see Refs. [23,24]). The leading-order $(\alpha_s \ln(1/x))^n$ terms result in a power-like growth, $x^{-\omega}$ with $\omega = (12\alpha_s \ln 2)/\pi$, at asymptotic values of $\ln\ 1/x$. More recently, the next-to-leading $\ln\ 1/x$ (NLLx) contributions have become available [25,26]. They are so large (and negative) that the result appears to be perturbatively unstable. Methods, based on a combination of collinear and small-x resummations, have been developed which reorganize the perturbative series into a more stable hierarchy [27–30]. There are indications that small-x resummations become necessary for sufficient precision for $x \lesssim 10^{-3}$ at low scales. On the other hand, there is no convincing indication for a 'non-linear' regime, for $Q^2 \gtrsim 2$ GeV^2, in which the gluon density would be so high that gluon-gluon recombination effects would become significant.

The precision of the experimental data demands that at least NLO, and preferably NNLO, DGLAP evolution be used in comparisons between QCD theory and experiment. Beyond the leading order, it is necessary to specify, and to use consistently, both a renormalization and a factorization scheme. The renormalization scheme used almost universally is the modified minimal subtraction ($\overline{\rm MS}$) scheme [31,32]. There are two popular choices for factorization scheme, in which the form of the correction for each structure function is different. The most-used factorization scheme is again $\overline{\rm MS}$ [33]. However, sometimes the DIS [34] scheme is adopted, in which there are no higher-order corrections to the F_2 structure function. The two schemes differ in how the non-divergent pieces are assimilated in the parton distribution functions.

The discussion above relates to the Q^2 behavior of leading-twist (twist-2) contributions to the structure functions. Higher-twist terms, which involve their own non-perturbative input, exist. These die off as powers of Q; specifically twist-n terms are damped by $1/Q^{n-2}$. Provided a cut, say $W^2 > 15$ GeV^2 is imposed, the higher-twist terms appear to be numerically unimportant for Q^2 above a few GeV^2, except for x close to 1 [35–37].

19.3. Determination of parton distributions

The parton distribution functions (PDFs) can be determined from an analysis of data for deep inelastic lepton-nucleon scattering and for related hard-scattering processes initiated by nucleons; see [38–42] for reviews. Table 19.1 highlights some of the processes, and their primary sensitivity to PDFs. The kinematic reach of fixed-target and collider experiments are complementary (as is shown in Fig. 19.3), which enables the determination of PDFs over a wide range in x and Q^2. As more precise LHC data for J/ψ, $W^{\pm}$, Z, γ, jet, $b\bar{b}$ and $t\bar{t}$ production become available, tighter constraints on the PDFs are expected in a wider kinematic range.

Recent determinations of the unpolarized PDFs up to NNLO have been made by six groups: MSTW [43,44], NNPDF [45], CT(EQ) [46], HERAPDF [13], ABM [47] and

Table 19.1: The main processes relevant to global PDF analyses, ordered in three groups: fixed-target experiments, HERA and the $p\bar{p}$ Tevatron / pp LHC. For each process we give an indication of their dominant partonic subprocesses, the primary partons which are probed and the approximate range of x constrained by the data.

Process	Subprocess	Partons	x range
$\ell^\pm \{p,n\} \to \ell^\pm X$	$\gamma^* q \to q$	$q, \bar{q}, g$	$x \gtrsim 0.01$
$\ell^\pm n/p \to \ell^\pm X$	$\gamma^* d/u \to d/u$	d/u	$x \gtrsim 0.01$
$pp \to \mu^+\mu^- X$	$u\bar{u}, d\bar{d} \to \gamma^*$	$\bar{q}$	$0.015 \lesssim x \lesssim 0.35$
$pn/pp \to \mu^+\mu^- X$	$(u\bar{d})/(u\bar{u}) \to \gamma^*$	$\bar{d}/\bar{u}$	$0.015 \lesssim x \lesssim 0.35$
$\nu(\bar{\nu})\, N \to \mu^-(\mu^+)\, X$	$W^* q \to q'$	$q, \bar{q}$	$0.01 \lesssim x \lesssim 0.5$
$\nu\, N \to \mu^-\mu^+\, X$	$W^* s \to c$	s	$0.01 \lesssim x \lesssim 0.2$
$\bar{\nu}\, N \to \mu^+\mu^-\, X$	$W^* \bar{s} \to \bar{c}$	$\bar{s}$	$0.01 \lesssim x \lesssim 0.2$
$e^\pm p \to e^\pm X$	$\gamma^* q \to q$	$g, q, \bar{q}$	$10^{-4} \lesssim x \lesssim 0.1$
$e^+ p \to \bar{\nu}\, X$	$W^+ \{d,s\} \to \{u,c\}$	d, s	$x \gtrsim 0.01$
$e^\pm p \to e^\pm\, c\bar{c} X, e^\pm\, b\bar{b} X$	$\gamma^* c \to c$, $\gamma^* g \to c\bar{c}$	c, b, g	$10^{-4} \lesssim x \lesssim 0.01$
$e^\pm p \to$ jet$+X$	$\gamma^* g \to q\bar{q}$	g	$0.01 \lesssim x \lesssim 0.1$
$p\bar{p}, pp \to$ jet$+X$	$gg, qg, qq \to 2j$	g, q	$0.005 \lesssim x \lesssim 0.5$
$p\bar{p} \to (W^\pm \to \ell^\pm\nu)\, X$	$ud \to W^+, \bar{u}\bar{d} \to W^-$	$u, d, \bar{u}, \bar{d}$	$x \gtrsim 0.05$
$pp \to (W^\pm \to \ell^\pm\nu)\, X$	$u\bar{d} \to W^+, d\bar{u} \to W^-$	$u, d, \bar{u}, \bar{d}, g$	$x \gtrsim 0.001$
$p\bar{p}(pp) \to (Z \to \ell^+\ell^-)X$	$uu, dd, ..(u\bar{u}, ..) \to Z$	$u, d, ..(g)$	$x \gtrsim 0.001$
$pp \to W^- c,\ W^+\bar{c}$	$gs \to W^- c$	$s, \bar{s}$	$x \sim 0.01$
$pp \to (\gamma^* \to \ell^+\ell^-)X$	$u\bar{u}, d\bar{d}, .. \to \gamma^*$	$\bar{q}, g$	$x \gtrsim 10^{-5}$
$pp \to b\bar{b}\, X, \quad t\bar{t} X$	$gg \to b\bar{b}, \quad t\bar{t}$	g	$x \gtrsim 10^{-5}, 10^{-2}$
$pp \to$ exclusive $J/\psi,\ \Upsilon$	$\gamma^*(gg) \to J/\psi,\ \Upsilon$	g	$x \gtrsim 10^{-5}, 10^{-4}$
$pp \to \gamma\, X$	$gq \to \gamma q$, $g\bar{q} \to \gamma\bar{q}$	g	$x \gtrsim 0.005$

GJR [48,49]. Most groups use input PDFs of the form $xf = x^a(...)(1-x)^b$ with 10-25 free parameters in total. Note, however, that the NNPDF group combines a Monte Carlo representation of the probability measure in the space of PDFs with the use of neural networks to give a set of unbiased input distributions, while GJR generate 'dynamical' PDFs from a valence-like input at a very low starting scale, $Q_0^2 = 0.5\ \text{GeV}^2$.

In these analyses the u, d and s quarks are taken to be massless, but the treatment of the heavy c and b quark masses, m_Q, differs, and has a long and chequered history, which may be traced from Refs. [50–61]. The MSTW, CT and NNPDF analyses use different variants of the General-Mass Variable-Flavour-Number Scheme (GM-VFNS). This combines fixed-order contributions to the coefficient functions (or partonic cross

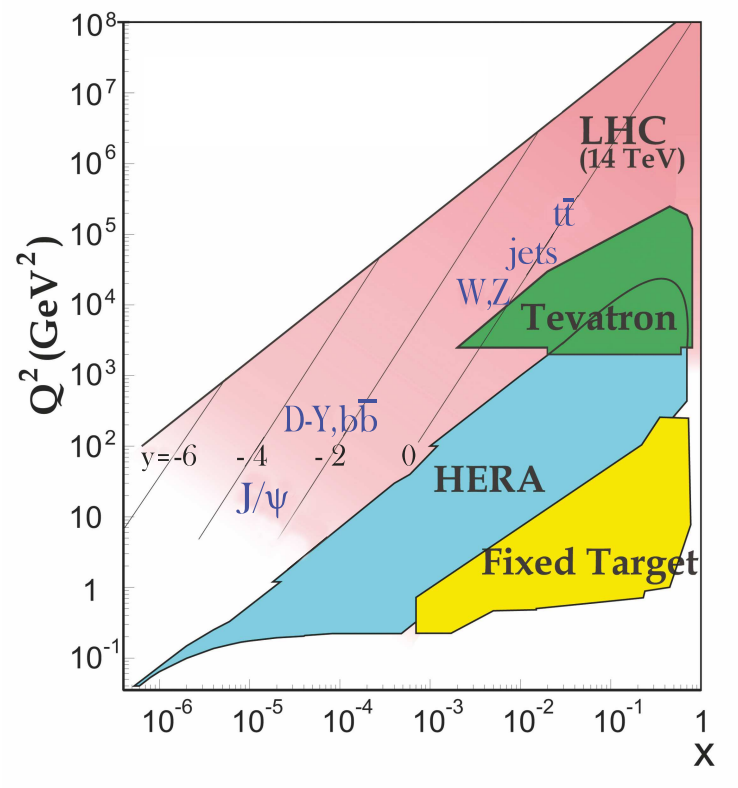

Figure 19.3: Kinematic domains in x and Q^2 probed by fixed-target and collider experiments. Some of the final states accessible at the LHC are indicated in the appropriate regions, where y is the rapidity. The incoming partons have $x_{1,2} = (M/14\ \text{TeV})e^{\pm y}$ with $Q = M$ where M is the mass of the state shown in blue in the figure. For example, exclusive J/ψ production at high $|y|$ at the LHC may probe the gluon PDF down to $x \sim 10^{-5}$.

sections) calculated with the full m_Q dependence, with the all-order resummation of contributions via DGLAP evolution in which the heavy quarks are treated as massless. The ABM analysis uses a FFNS where only the three light (massless) quarks enter the evolution, while the heavy quarks enter the partonic cross sections with their full m_Q dependence; transition matrix elements are computed, following [53], which provide the boundary conditions between n_f and n_f+1 PDFs. The GM-VFNS and FFNS approaches yield different results: in particular $\alpha_s(M_Z^2)$ and a large-x gluon PDF at large Q^2 are both significantly smaller in the FFNS. It has been argued [36,37,60] that the difference

is due to the slow convergence of the $\ln^n(Q^2/m_Q^2)$ terms in a FFNS.

The most recent determinations of the groups using GM-VFNS (MSTW, NNPDF and CT(EQ)) have converged, so that now a reasonable agreement has been achieved between the resulting PDFs, the value obtained for $\alpha_s(M_Z^2)$, and their predictions for the LHC. For illustration, we show in Fig. 19.4 the PDFs obtained in the NNLO NNPDF analysis [45] at scales $\mu^2 = 10$ and 10^4 GeV^2. The values of α_s found by MSTW [43,63] may be taken as representative of those resulting from the GM-VFNS analyses

$$\text{NLO} : \alpha_s(M_Z^2) = 0.1202^{+0.0012}_{-0.0015} \pm 0.003,$$

$$\text{NNLO} : \alpha_s(M_Z^2) = 0.1171 \pm 0.0014 \pm 0.002,$$

where the first error (at 68% C.L.) corresponds to the uncertainties resulting from the data fitted and the second is an estimate of the theory error (that is, the uncertainty that might be expected from the neglect of higher orders), see also [64]. The ABM analysis [47], which uses a FFNS, finds $\alpha_s(M_Z^2) = 0.1134 \pm 0.0011$ at NNLO.

Spin-dependent (or polarized) PDFs have been obtained through NLO global analyses which include measurements of the g_1 structure function in inclusive polarized DIS, 'flavour-tagged' semi-inclusive DIS data, and results from polarized pp scattering at RHIC. Recent NLO analyses are given in Refs. [65–68]. Improved parton-to-hadron fragmentation functions, needed to describe the semi-inclusive DIS data, can be found in [69–71]. Fig. 19.5 shows several global analyses at a scale of 2.5 GeV^2 along with the data from semi-inclusive DIS. A recent determination [72], using the NNPDF methodology, concentrates just on the inclusive polarized DIS data, and finds the errors on the polarized gluon PDF have been underestimated in the earlier analyses.

Comprehensive sets of PDFs are available as program-callable functions from the HepData website [78], which includes comparison graphics of PDFs, and from the LHAPDF library [79], which can be linked directly into a user's programme to provide access to recent PDFs in a standard format.

19.4. The hadronic structure of the photon

Besides the *direct* interactions of the photon, it is possible for it to fluctuate into a hadronic state via the process $\gamma \to q\overline{q}$. While in this state, the partonic content of the photon may be *resolved*, for example, through the process $e^+e^- \to e^+e^-\gamma^*\gamma \to e^+e^-X$, where the virtual photon emitted by the DIS lepton probes the hadronic structure of the quasi-real photon emitted by the other lepton. The perturbative LO contributions, $\gamma \to q\overline{q}$ followed by $\gamma^* q \to q$, are subject to QCD corrections due to the coupling of quarks to gluons.

Often the equivalent-photon approximation is used to express the differential cross section for deep inelastic electron–photon scattering in terms of the structure functions of the transverse quasi-real photon times a flux factor N_γ^T (for these incoming quasi-real photons of transverse polarization)

$$\frac{d^2\sigma}{dxdQ^2} = N_\gamma^T \frac{2\pi\alpha^2}{xQ^4}\left[\left(1+(1-y)^2\right)F_2^\gamma(x,Q^2) - y^2 F_L^\gamma(x,Q^2)\right],$$

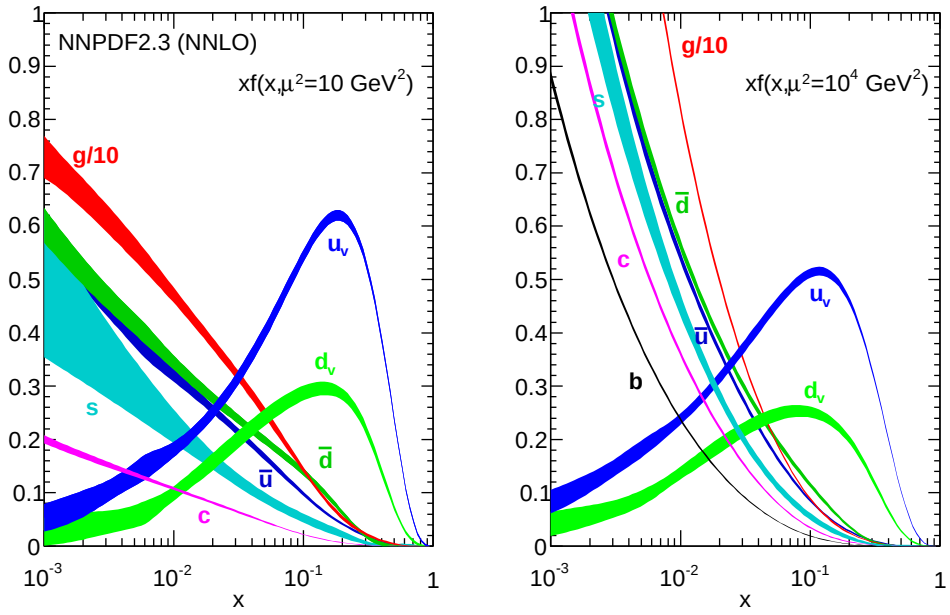

Figure 19.4: The bands are x times the unpolarized parton distributions $f(x)$ (where $f = u_v, d_v, \overline{u}, \overline{d}, s \simeq \bar{s}, c = \bar{c}, b = \bar{b}, g$) obtained in NNLO NNPDF2.3 global analysis [45] at scales $\mu^2 = 10$ GeV^2 and $\mu^2 = 10^4$ GeV^2, with $\alpha_s(M_Z^2) = 0.118$. The analogous results obtained in the NNLO MSTW analysis [43] can be found in Ref. [62].

where we have used $F_2^\gamma = 2xF_T^\gamma + F_L^\gamma$, not to be confused with F_2^γ of Sec. 19.2. Complete formulae are given, for example, in the comprehensive review of Ref. 80.

The hadronic photon structure function, F_2^γ, evolves with increasing Q^2 from the 'hadron-like' behavior, calculable via the vector-meson-dominance model, to the dominating 'point-like' behaviour, calculable in perturbative QCD. Due to the point-like coupling, the logarithmic evolution of F_2^γ with Q^2 has a *positive* slope for all values of x, see Fig. 19.15. The 'loss' of quarks at large x due to gluon radiation is over-compensated by the 'creation' of quarks via the point-like $\gamma \to q\bar{q}$ coupling. The logarithmic evolution was first predicted in the quark–parton model ($\gamma^*\gamma \to q\bar{q}$) [81,82], and then in QCD in the limit of large Q^2 [83]. The evolution is now known to NLO [84–86]. The NLO data analyses to determine the parton densities of the photon can be found in [87–89].

19.5. Diffractive DIS (DDIS)

Some 10% of DIS events are diffractive, $\gamma^* p \to X + p$, in which the slightly deflected proton and the cluster X of outgoing hadrons are well-separated in rapidity. Besides x and Q^2, two extra variables are needed to describe a DDIS event: the fraction $x_{I\!P}$ of the proton's momentum transferred across the rapidity gap and t, the square of the 4-momentum transfer of the proton. The DDIS data [90,91] are usually analyzed using two levels of factorization. First, the diffractive structure function F_2^{D} satisfies *collinear*

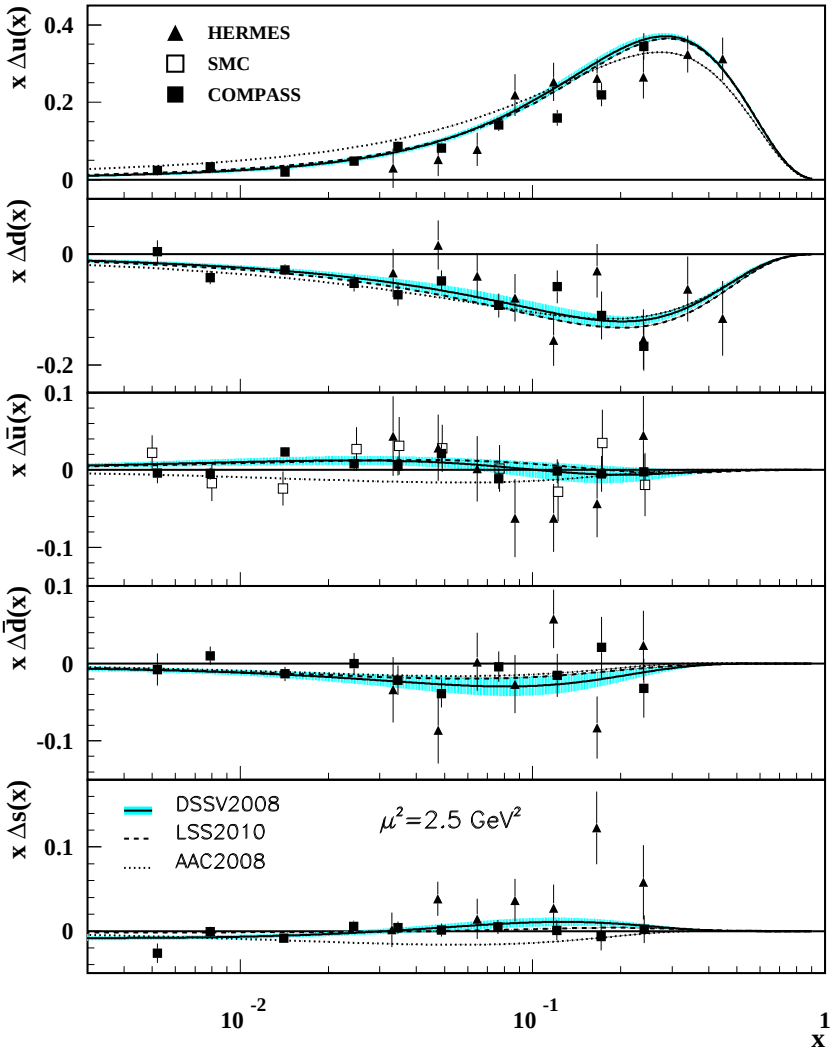

Figure 19.5: Distributions of x times the polarized parton distributions $\Delta q(x)$ (where $q = u, d, \overline{u}, \overline{d}, s$) using the AAC2008 [65], DSSV2008 [66], and LSS2010 [68] parameterizations at a scale $\mu^2 = 2.5$ GeV^2, showing the blue-shaded error corridor of the DSSV2008 set (corresponding to a one-unit increase in χ^2) (see also BB2010 [67]) . The points represent data from semi-inclusive positron (HERMES [73,74]) and muon (SMC [75] and COMPASS [76,77]) deep inelastic scattering given at $Q^2 = 2.5$ GeV^2. The SMC results are extracted under the assumption that $\Delta\overline{u}(x) = \Delta\overline{d}(x)$.

factorization, and can be expressed as the convolution [92]

$$F_2^{\mathrm{D}} = \sum_{a=q,g} C_2^a \otimes f_{a/p}^{\mathrm{D}}, \tag{19.31}$$

with the same coefficient functions as in DIS (see Eq. (19.21)), and where the diffractive parton distributions $f^{\rm D}_{a/p}$ $(a = q, g)$ satisfy DGLAP evolution. Second, *Regge factorization* is assumed [93],

$$f^{\rm D}_{a/p}(x_{I\!P}, t, z, \mu^2) = f_{I\!P/p}(x_{I\!P}, t)\, f_{a/I\!P}(z, \mu^2), \tag{19.32}$$

where $f_{a/I\!P}$ are the parton densities of the Pomeron, which itself is treated like a hadron, and $z \in [x/x_{I\!P}, 1]$ is the fraction of the Pomeron's momentum carried by the parton entering the hard subprocess. The Pomeron flux factor $f_{I\!P/p}(x_{I\!P}, t)$ is taken from Regge phenomenology. There are also secondary Reggeon contributions to Eq. (19.32). A sample of the t-integrated diffractive parton densities, obtained in this way, is shown in Fig. 19.6.

Although collinear factorization holds as $\mu^2 \to \infty$, there are non-negligible corrections for finite μ^2 and small $x_{I\!P}$. Besides the *resolved* interactions of the Pomeron, the perturbative QCD Pomeron may also interact *directly* with the hard subprocess, giving rise to an inhomogeneous evolution equation for the diffractive parton densities analogous to the photon case. The results of the MRW analysis [96], which includes these contributions, are also shown in Fig. 19.6. Unlike the inclusive case, the diffractive parton densities cannot be directly used to calculate diffractive hadron-hadron cross sections, since account must first be taken of "soft" rescattering effects.

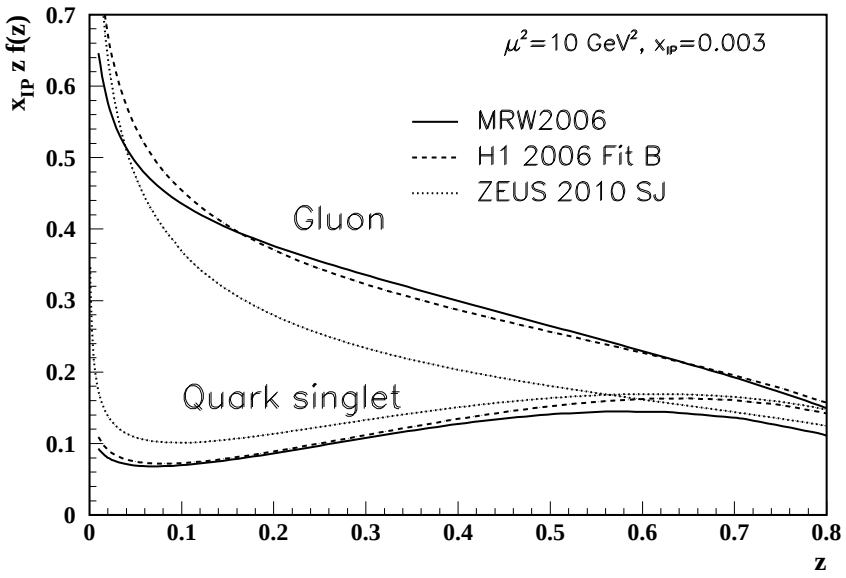

Figure 19.6: Diffractive parton distributions, $x_{I\!P}\, z f^{\rm D}_{a/p}$, obtained from fitting to the ZEUS data with $Q^2 > 5$ GeV^2 [94], H1 data with $Q^2 > 8.5$ GeV^2 assuming Regge factorization [95], and from MRW2006 [96] using a more perturbative QCD approach [96]. Only the Pomeron contributions are shown and not the secondary Reggeon contributions, which are negligible at the value of $x_{I\!P} = 0.003$ chosen here. The H1 2007 Jets distribution [97] is similar to H1 2006 Fit B.

19.6. Generalized parton distributions

The parton distributions of the proton of Sec. 19.3 are given by the diagonal matrix elements $\langle P,\lambda|\hat{O}|P,\lambda\rangle$, where P and λ are the 4-momentum and helicity of the proton, and $\hat{O}$ is a twist-2 quark or gluon operator. However, there is new information in the so-called generalised parton distributions (GPDs) defined in terms of the off-diagonal matrix elements $\langle P',\lambda'|\hat{O}|P,\lambda\rangle$; see [98–102] for reviews. Unlike the diagonal PDFs, the GPDs cannot be regarded as parton densities, but are to be interpreted as probability amplitudes.

The physical significance of GPDs is best seen using light-cone coordinates, $z^{\pm}=(z^0\pm z^3)/\sqrt{2}$, and in the light-cone gauge, $A^+=0$. It is conventional to define the generalised quark distributions in terms of quark operators at light-like separation

$$F_q(x,\xi,t) \;=\; \frac{1}{2}\int\frac{dz^-}{2\pi}\;e^{ix\bar{P}^+z^-}\;\langle P'|\bar{\psi}(-z/2)\gamma^+\psi(z/2)|P\rangle\;\Big|_{z^+=z^1=z^2=0} \tag{19.33}$$

$$=\frac{1}{2\bar{P}^+}\left(H_q(x,\xi,t)\;\bar{u}(P')\gamma^+u(P)\;+\;E_q(x,\xi,t)\;\bar{u}(P')\frac{i\sigma^{+\alpha}\Delta_\alpha}{2m}u(P)\right) \tag{19.34}$$

with $\bar{P}=(P+P')/2$ and $\Delta=P'-P$, and where we have suppressed the helicity labels of the protons and spinors. We now have two extra kinematic variables:

$$t=\Delta^2, \qquad \xi=-\Delta^+/(P+P')^+. \tag{19.35}$$

We see that $-1\le\xi\le 1$. Similarly, we may define GPDs $\tilde{H}_q$ and $\tilde{E}_q$ with an additional γ_5 between the quark operators in Eq. (19.33); and also an analogous set of gluon GPDs, $H_g,\;E_g,\;\tilde{H}_g$ and $\tilde{E}_g$. After a Fourier transform with respect to the transverse components of Δ, we are able to describe the spatial distribution of partons in the impact parameter plane in terms of GPDs [103,104].

For $P'=P,\;\lambda'=\lambda$ the matrix elements reduce to the ordinary PDFs of Sec. 19.2.1

$$H_q(x,0,0)=q(x), \qquad H_q(-x,0,0)=-\bar{q}(x), \qquad H_g(x,0,0)=xg(x), \tag{19.36}$$

$$\tilde{H}_q(x,0,0)=\Delta q(x), \qquad \tilde{H}_q(-x,0,0)=\Delta\bar{q}(x), \qquad \tilde{H}_g(x,0,0)=x\Delta g(x), \tag{19.37}$$

where $\Delta q=q\uparrow-q\downarrow$ as in Eq. (19.18). No corresponding relations exist for $E,\;\tilde{E}$ as they decouple in the forward limit, $\Delta=0$.

The functions H_g,E_g are even in x, and $\tilde{H}_g,\tilde{E}_g$ are odd functions of x. We can introduce valence and 'singlet' quark distributions which are even and odd functions of x respectively. For example

$$H_q^V(x,\xi,t)\equiv H_q(x,\xi,t)+H_q(-x,\xi,t)=H_q^V(-x,\xi,t), \tag{19.38}$$

$$H_q^S(x,\xi,t)\equiv H_q(x,\xi,t)-H_q(-x,\xi,t)=-H_q^S(-x,\xi,t). \tag{19.39}$$

All the GPDs satisfy relations of the form

$$H(x,-\xi,t) = H(x,\xi,t) \qquad \text{and} \qquad H(x,-\xi,t)^* = H(x,\xi,t), \tag{19.40}$$

and so are real-valued functions. Moreover, the moments of GPDs, that is the x integrals of $x^n H_q$ etc., are *polynomials* in ξ of order $n+1$. Another important property of GPDs are Ji's sum rules [98]

$$\frac{1}{2}\int_{-1}^{1} dx \;\; x\left(H_q(x,\xi,t) + E_q(x,\xi,t)\right) = J_q(t), \tag{19.41}$$

where $J_q(0)$ is the total angular momentum carried by quarks and antiquarks of flavour q, with a similar relation for gluons.

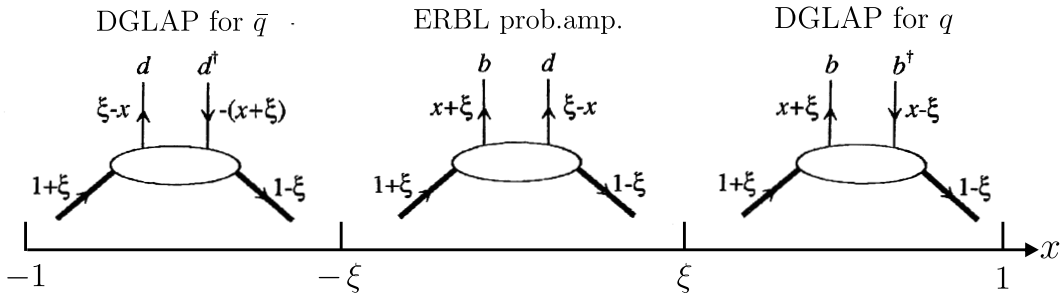

Figure 19.7: Schematic diagrams of the three distinct kinematic regions of the imaginary part of H_q. The proton and quark momentum fractions refer to $\bar{P}^+$, and x covers the interval (-1,1). In the ERBL domain the GPDs are generalisations of distribution amplitudes which occur in processes such as $p\bar{p} \to J/\psi$.

To visualize the physical content of H_q, we Fourier expand ψ and $\bar{\psi}$ in terms of quark, antiquark creation (b, d) and annihilation $(b^\dagger, d^\dagger)$ operators, and sketch the result in Fig. 19.7. There are two types of domain: (i) the time-like or 'annihilation' domain, with $|x| < |\xi|$, where the GPDs describe the wave functions of a t-channel $q\bar{q}$ (or gluon) pair and evolve according to modified ERBL equations [105,106]; (ii) the space-like or 'scattering' domain, with $|x| > |\xi|$, where the GPDs generalise the familiar $\bar{q}$, q (and gluon) PDFs and describe processes such as 'deeply virtual Compton scattering' $(\gamma^* p \to \gamma p)$, $\gamma p \to J/\psi p$, etc., and evolve according to modified DGLAP equations. The splitting functions for the evolution of GPDs are known to NLO [107].

GPDs describe new aspects of proton structure and must be determined from experiment. We can parametrise them in terms of 'double distributions' [108,109], which reduce to diagonal PDFs as $\xi \to 0$. With an additional physically reasonable 'Regge' assumption of no extra singularity at $\xi = 0$, GPDs at low ξ are uniquely given in terms of diagonal PDFs to $O(\xi)$, and have been used [110] to describe $\gamma p \to J/\psi p$ data.

Alternatively, flexible $SO(3)$-based parametrisations have been used to determine GPDs from DVCS data [111].

---

* The value of $\eta^{\rm CC}$ deduced from Ref. 1 is found to be a factor of two too small; $\eta^{\rm CC}$ of Eq. (19.9) agrees with Refs. [2,3].

References:

1. J. Blümlein and N. Kochelev, Nucl. Phys. **B498**, 285 (1997).
2. S. Forte *et al.*, Nucl. Phys. **B602**, 585 (2001).
3. M. Anselmino *et al.*, Z. Phys. **C64**, 267 (1994).
4. M. Anselmino *et al.*, Phys. Rep. **261**, 1 (1995).
5. M. Klein and T. Riemann, Z. Phys. **C24**, 151 (1984).
6. C.G. Callan and D.J. Gross, Phys. Rev. Lett. **22**, 156 (1969).
7. D.A. Dicus, Phys. Rev. **D5**, 1367 (1972).
8. J.D. Bjorken and E.A. Paschos, Phys. Rev. **185**, 1975 (1969).
9. R.P. Feynman, Photon Hadron Interactions (Benjamin, New York, 1972).
10. S. Wandzura and F. Wilczek, Phys. Rev. **B72**, 195 (1977).
11. J. Blümlein and A. Tkabladze, Nucl. Phys. **B553**, 427 (1999).
12. J.D. Bjorken, Phys. Rev. **179**, 1547 (1969).
13. V. Radescu for the H1 and ZEUS Collaborations, `arXiv:1308.0374`.
14. V.N. Gribov and L.N. Lipatov, Sov. J. Nucl. Phys. **15**, 438 (1972).
15. L.N. Lipatov, Sov. J. Nucl. Phys. **20**, 95 (1975).
16. G. Altarelli and G. Parisi, Nucl. Phys. **B126**, 298 (1977).
17. Yu.L. Dokshitzer, Sov. Phys. JETP **46**, 641 (1977).
18. G. Curci *et al.*, Nucl. Phys. **B175**, 27 (1980); W. Furmanski, and R. Petronzio, Phys. Lett. **B97**, 437 (1980).
19. R.K. Ellis *et al.*, QCD and Collider Physics (Cambridge UP, 1996).
20. E.B. Zijlstra and W.L. van Neerven, Phys. Lett. **B272**, 127 (1991); Phys. Lett. **B273**, 476 (1991); Phys. Lett. **B297**, 377 (1992); Nucl. Phys. **B383**, 525 (1992).
21. S. Moch and J.A.M. Vermaseren, Nucl. Phys. **B573**, 853 (2000).
22. S. Moch *et al.*, Nucl. Phys. **B688**, 101 (2004); Nucl. Phys. **B691**, 129 (2004); Phys. Lett. **B606**, 123 (2005); Nucl. Phys. **B724**, 3 (2005).
23. E.A. Kuraev *et al.*, Phys. Lett. **B60**, 50 (1975); Sov. Phys. JETP **44**, 443 (1976); Sov. Phys. JETP **45**, 199 (1977).
24. Ya.Ya. Balitsky and L.N. Lipatov, Sov. J. Nucl. Phys. **28**, 822 (1978).
25. V.S. Fadin, and L.N. Lipatov, Phys. Lett. **B429**, 127 (1998).
26. G. Camici and M. Ciafaloni, Phys. Lett. **B412**, 396 (1997), erratum-Phys. Lett. **B147**, 390 (1997); Phys. Lett. **B430**, 349 (1998).
27. M. Ciafaloni *et al.*, Phys. Rev. **D60**, 114036 (1999); JHEP **0007** 054 (2000).
28. M. Ciafaloni *et al.*, Phys. Lett. **B576**, 143 (2003); Phys. Rev. **D68**, 114003 (2003).
29. G. Altarelli *et al.*, Nucl. Phys. **B742**, 1 (2006); Nucl. Phys. **B799**, 199 (2008).
30. C.D. White and R.S. Thorne, Phys. Rev. **D75**, 034005 (2007).
31. G. 't Hooft and M. Veltman, Nucl. Phys. **B44**, 189 (1972).
32. G. 't Hooft, Nucl. Phys. **B61**, 455 (1973).
33. W.A. Bardeen *et al.*, Phys. Rev. **D18**, 3998 (1978).

34. G. Altarelli *et al.*, Nucl. Phys. **B143**, 521 (1978) and erratum: Nucl. Phys. **B146**, 544 (1978).
35. A.D. Martin *et al.*, Eur. Phys. J. **C35**, 325 (2004).
36. NNPDF, R.D. Ball *et al.*, Phys. Lett. **B723**, 330 (2013).
37. R.S. Thorne arXiv:1306.3907.
38. A. De Roeck and R.S. Thorne, Prog. in Part. Nucl. Phys. **66**, 727 (2011).
39. S. Forte and G. Watt, Ann.Rev.Nucl.Part.Sci. **63**; arXiv:1301.6754.
40. J. Blumlein, Prog. in Part. Nucl. Phys. **69**, 28 (2013).
41. E. Perez and E. Rizvi, Rept. on Prog. in Phys. **76**, 046201 (2013).
42. R.D. Ball *et al.*, JHEP **1304**, 125 (2013).
43. MSTW, A.D. Martin *et al.*, Eur. Phys. J. **C63**, 189 (2009).
44. A.D. Martin *et al.*, Eur. Phys. J. **C73**, 2318 (2013).
45. NNPDF, R.D. Ball *et al.*, Nucl. Phys. **B867**, 244 (2013).
46. CT10, Jun Gao *et al.*, arXiv:1302.6246.
47. S. Alekhin, *et al.*, Phys. Rev. **D86**, 054009 (2012).
48. M. Glück *et al.*, Eur. Phys. J. **C53**, 355 (2008).
49. P. Jimenez-Delgado and E. Reya, Phys. Rev. **D79**, 074023 (2009).
50. J.C. Collins, F. Wilczek, and A. Zee, Phys. Rev. **D18**, 242 (1978).
51. E. Laenen *et al.*, Nucl. Phys. **B392**, 162 (1993).
52. M.A.G. Aivazis *et al.*, Phys. Rev. **D50**, 3102 (1994).
53. M. Buza *et al.*, Eur. Phys. J. **C1**, 301 (1998).
54. A. Chuvakin *et al.*, Phys. Rev. **D61**, 096004 (2000).
55. S. Kretzer *et al.*, Phys. Rev. **D69**, 114005 (2004).
56. R.S. Thorne, Phys. Rev. **D73**, 054019 (2006).
57. R.S. Thorne and W.-K. Tung, Proc. 4th HERA-LHC Workshop, arXiv:0809.0714.
58. S. Alekhin and S. Moch, Phys. Lett. **B699**, 345 (2011).
59. S. Forte *et al.*, Nucl. Phys. **B834**, 116 (2010).
60. R.S. Thorne, Phys. Rev. **D86**, 074017 (2012).
61. E.G. de Oliveira *et al.*, Eur. Phys. J. **C73**, 2616 (2013).
62. J. Beringer *et al.*, (PDG), Phys. Rev. **D86**, 010001 (2012).
63. MSTW, A.D. Martin *et al.*, Eur. Phys. J. **C64**, 653 (2009).
64. NNPDF, R.D. Ball *et al.*, Phys. Lett. **B701**, 346 (2011).
65. M. Hirai *et al.*, Nucl. Phys. **B813**, 106 (2009).
66. D. de Florian *et al.*, Phys. Rev. Lett. **101**, 072001 (2008); Phys. Rev. **D80**, 034030 (2009).
67. J. Blümlein and H. Böttcher, Nucl. Phys. **B841**, 205 (2010).
68. E. Leader *et al.*, Phys. Rev. **D82**, 114018 (2010).
69. D. de Florian *et al.*, Phys. Rev. **D75**, 114010 (2007); Phys. Rev. **D76**, 074033 (2007).
70. S. Albino *et al.*, Nucl. Phys. **B803**, 42 (2008).
71. M. Hirai and S. Kumano, Comp. Phys. Comm. **183**, 1002 (2012).
72. NNPDF, R.D. Ball *et al.*, Nucl. Phys. **B874**, 36 (2013).
73. HERMES, A. Airpetian *et al.*, Phys. Rev. Lett. **92**, 012005 (2004); A. Airpetian *et al.*, Phys. Rev. **D71**, 012003 (2005).

74. HERMES, A. Airpetian *et al.*, Phys. Lett. **B666**, 446 (2008).
75. SMC, B. Adeva *et al.*, Phys. Lett. **B420**, 180 (1998).
76. COMPASS, M. Alekseev *et al.*, Phys. Lett. **B680**, 217 (2009).
77. COMPASS, M. Alekseev *et al.*, Phys. Lett. **B693**, 227 (2010).
78. `http://hepdata.cedar.ac.uk/pdfs`.
79. `http://lhapdf.hepforge.org/`.
80. R. Nisius, Phys. Reports **332**, 165 (2000).
81. T.F. Walsh and P.M. Zerwas, Phys. Lett. **B44**, 195 (1973).
82. R.L. Kingsley, Nucl. Phys. **B60**, 45 (1973).
83. E. Witten, Nucl. Phys. **B120**, 189 (1977).
84. W.A. Bardeen and A.J. Buras, Phys. Rev. **D20**, 166 (1979), erratum Phys. Rev. **D21**, 2041 (1980).
85. M. Fontannaz and E. Pilon, Phys. Rev. **D45**, 382 (1992), erratum Phys. Rev. **D46**, 484 (1992).
86. M. Glück *et al.*, Phys. Rev. **D45**, 3986 (1992).
87. F. Cornet *et al.*, Phys. Rev. **D70**, 093004 (2004).
88. P. Aurenche, *et al.*, Eur. Phys. J. **C44**, 395 (2005).
89. W. Slominski *et al.*, Eur. Phys. J. **C45**, 633 (2006).
90. H1+ZEUS, F.D. Aaron *et al.*, Eur. Phys. J. **C72**, 2175 (2012).
91. H1, F.D. Aaron *et al.*, Eur. Phys. J. **C72**, 2074 (2012).
92. J.C. Collins, Phys. Rev. **D57**, 3051 (1998); Erratum Phys. Rev. **D61**, 019902 (2000).
93. G. Ingelman and P. E. Schlein, Phys. Lett. **B152**, 256 (1985).
94. ZEUS, S. Chekanov *et al.*, Nucl. Phys. **B831**, 1 (2010).
95. H1, A. Aktas *et al.*, Eur. Phys. J. **C48**, 715 (2006).
96. A.D. Martin, M.G. Ryskin, and G. Watt, Phys. Lett. **B644**, 131 (2007).
97. H1, A. Aktas *et al.*, JHEP **0710**, 042 (2007).
98. X. Ji, J. Phys. **G24**, 1181 (1998).
99. K. Goeke *et al.*, Prog. in Part. Nucl. Phys. **47**, 401 (2001).
100. M. Diehl, Phys. Rept. **388**, 41 (2003).
101. A.V. Belitsky and A.V. Radyushkin, Phys. Rept. **418**, 1 (2005).
102. S. Boffi and B. Pasquini, Riv. Nuovo Cimento **30**, 387 (2007).
103. M. Burkardt, Int. J. Mod. Phys. **A18**, 173 (2003).
104. M. Diehl, Eur. Phys. J. **C25**, 223 (2002).
105. A.V. Efremov and A.V. Radyushkin, Phys. Lett. **B94**, 245 (1980).
106. G.P. Lepage and S.J. Brodsky, Phys. Rev. **D22**, 2157 (1980).
107. A.V. Belitsky *et al.*, Phys. Lett. **B493**, 341 (2000).
108. A.V. Radyushkin, Phys. Rev. **D59**, 014030 (1999).
109. A.V. Radyushkin, Phys. Lett. **B449**, 81 (1999).
110. A.D. Martin *et al.*, Eur. Phys. J. **C63**, 57 (2009).
111. K. Kumerički and D. Müller, Nucl. Phys. **B841**, 1 (2010).